Phase Transitions in Lanthanum-Doped Strontium Bismuth Tantalate

Karl R. Whittle,* Neil C. Hyatt, and Ian M. Reaney

Ceramics and Composites Laboratory Department of Engineering Materials, University of Sheffield, Mappin Street, Sheffield S1 3JD, United Kingdom

Received February 18, 2008. Revised Manuscript Received August 21, 2008

The effect of lanthanum substitution for bismuth in the Aurivillius phase, $SrBi_{2-x}La_xTa_2O_9$ ($x = 0$, 0.01, 0.02, 0.05, 0.1, 0.15, and 0.2) has been investigated. Increasing La concentration decreased the ferroelectric−paraelectric ($A2_1am$−Amam) transformation temperature until by $x = 0.15$, the material was paraelectric at room temperature. The transformation from $A2_1am$ to Amam (T_{A21am}) was difficult to observe by neutron and X-ray diffraction but could be monitored using Raman spectroscopy for which unique modes associated with the loss of centrosymmetry were identified in the ferroelectric phase. Although the effect of La substitution for Bi on the I4/mmm−Amam (T_{Amam}) phase transition is difficult to monitor, the intensity of the superstructure reflections in ED patterns obtained at room temperature remained qualitatively similar regardless of La concentration. La substitution was therefore considered to expand the $T_{Amam}-T_{A21am}$ temperature interval.

Introduction

Strontium bismuth tantalate (SBT) is a member of the Aurivillius family [1−3] of layered ceramics $(Bi_2O_2)^{2+}[A_{n-1}B_nO_{3n+1}]$, for which $n = 2$.[4,5] Aurivillius layered materials may be considered as alternating layers of strontium bismuth tantalate $SrTa_2O_7^{2-}$ perovskite blocks interleaved with layers of $Bi_2O_2^{2+}$. SBT is ferroelectric at room temperature with $A2_1am$ symmetry but on heating to >573 K it undergoes a continuous transition to a paraelectric Amam[6] phase and at ~823 K[7] it undergoes a transition to the prototype I4/mmm phase. Schematics of the crystal structure are shown in Figure 1. Essentially, the $A2_1am$ phase is noncentrosymmetric with parallel cation displacements giving rise to spontaneous polarization that are coupled to in-phase rotations of the O octahedra around the *b* and *c* axes, whereas the Amam phase is centrosymmetric with in phase rotations of O octahedra only around the *b* axis. The I4/mmm phase is the prototype structure which is centrosymmetric and untilted. The in-phase rotations in the Amam and $A2_1am$ phases double the unit cell with respect to I4/mmm but despite a difference in symmetry the reflection conditions for Amam and $A2_1am$ are identical.[6,7] The presence of intermediate paraelectric phases with doubled unit cells in Aurivillius compounds was first established by Reaney et al.[8] using in situ electron diffraction in strontium bismuth titanate ceramics. Subsequently, Hervoches and Lightfoot[7]used high-temperature neutron data to refine an Amam cell in $SrBi_2Ta_2O_9$.

Previous studies[9] have demonstrated that SBT has a high remanent polarization, low coercive field, and an absence of ferroelectric fatigue. Such properties make SBT an ideal candidate for nonvolatile ferroelectric memories (NVFRAM).[10,11] As a result, extensive research has been undertaken using a combination of neutron diffraction at variable temperature,[12−14] electron microscopy, and Raman spectroscopy[5] to determine structure−property relations in this system. Macquart et al. [12] confirmed the existence of the Amam phase at temperatures above 650 K, but has suggested that there is a continuous transition to I4/mmm symmetry between 650 and 800 K. The presence of a distorted phase at temperatures higher than 650 K was also confirmed by Kamba et al. [15] who observed ferroelastic domains in strontium bismuth tantalate up to 770 K.

Doping with lanthanide (Ln^{3+}) ions has been investigated but commonly, substitution for Sr has been attempted in order to donor dope SBT in a manner reminiscent of soft

* Corresponding author. Current address: Institute of Materials Engineering, Australian Nuclear Science and Technology Organisation, PMB 1, Menai, NSW 2234, Australia. E-mail: karl.whittle@ansto.gov.au.

(1) Aurivillius, B. *Ark. Kemi.* **1950**, *2*, 519–27.
(2) Aurivillius, B. *Ark. Kemi.* **1949**, *1*, 499–512.
(3) Aurivillius, B. *Ark. Kemi.* **1949**, *1*, 463–80.
(4) Suarez, D. Y.; Reaney, I. M.; Lee, W. E. *J. Mater. Res.* **2001**, *16*, 3139–3149.
(5) Graves, P. R.; Hua, G.; Myhra, S.; Thompson, J. G. *J. Solid State Chem.* **1995**, *114*, 112–122.
(6) Almeida, A.; Chaves, M. R.; Amorin, H.; Costa, M. E. V.; Kholkin, A. L. *J. Phys.: Condens. Matter* **2005**, *17*, 7605–7612.
(7) Hervoches, C. H.; Irvine, J. T. S.; Lightfoot, P. *Phys. Rev. B* **2001**, 6410.
(8) Reaney, I. M.; Roulin, M.; Shulman, H. S.; Setter, N. *Ferroelectrics* **1995**, *165*, 295–305.
(9) de Araujo, C. A. P.; Cuchiaro, J. D.; McMillan, L. D.; Scott, M. C.; Scott, J. F. *Nature (London)* **1995**, *374*, 627–9.
(10) Perez-Mato, J. M.; Aroyo, M.; Garcia, A.; Blaha, P.; Schwarz, K.; Schweifer, J.; Parlinski, K. *Phys. Rev. B* **2004**, 70.
(11) Das, R. R.; Perez, W.; Katiyar, R. S. *Integr. Ferroelectr.* **2001**, *37*, 295–304.
(12) Macquart, R.; Kennedy, B. J.; Hunter, B. A.; Howard, C. J.; Shimakawa, Y. *Integr. Ferroelectr.* **2002**, *44*, 101–112.
(13) Macquart, R.; Kennedy, B. J.; Shimakawa, Y. *J. Solid State Chem.* **2001**, *160*, 174–177.
(14) Macquart, R.; Kennedy, B. J.; Kubota, Y.; Nisibori, E.; Takata, M. *Ferroelectrics* **2000**, *248*, 27–32.
(15) Kamba, S.; Pokorny, J.; Porokhonskyy, V.; Petzelt, J.; Moret, M. P.; Garg, A.; Barber, Z. H.; Zallen, R. *Appl. Phys. Lett.* **2002**, *81*, 1056–1058.

10.1021/cm800475z CCC: $40.75
Published on Web 09/24/2008

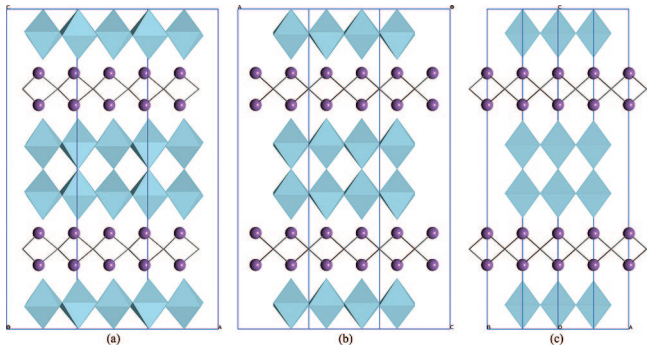

Figure 1. Unit cell images of $SrBi_2Ta_2O_9$ with (a) $A2_1am$, (b) Amam, and (c) I4/mmm symmetries along the [100] direction. The polyhedra indicate the TaO_6 octahedra; the Bi_2O_2 layers are shown as ions.

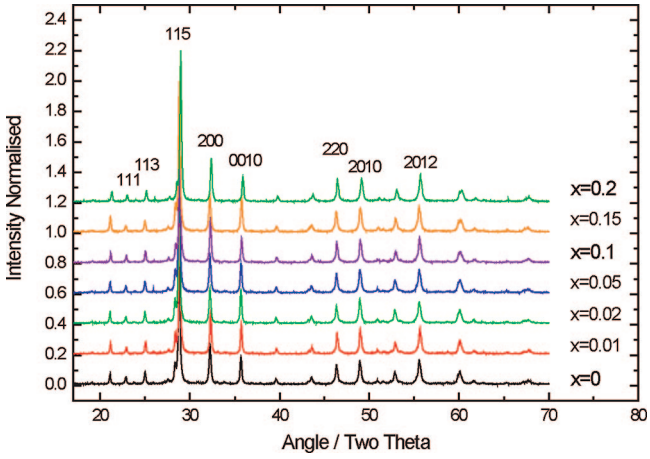

Figure 2. X-ray diffraction patterns recorded from calcined powders. No second phases are observed and there is no significant difference between the spectra.

$Pb(Zr,TiO)_3$.[16−19] This mechanism has been shown to lower the ferroelectric T_c from ∼300 to 180 °C when, e.g., Sr^{2+} was exchanged[20] with Pr^{3+}. The aim of this current work is to examine the effects of doping for Bi^{3+} with isovalent La^{3+} using the substitutional formula, $SrBi_{2-x}La_xTa_2O_9$. The ceramics were examined using electron microscopy, neutron diffraction and variable-temperature Raman spectroscopy in order to provide complementary information about the structure and allow more complete interpretation of the dielectric and ferroelectric properties.

Experimental Section

Samples were prepared by the calcination of stoichiometric amounts of $SrCO_3$ (99%, Aldrich), Bi_2O_3 (99.5%, Aldrich), Ta_2O_5 (99.9%, Aldrich), and La_2O_3 (99.5%, Aldrich). The powders were ball-milled using yttrium-stabilized zirconia milling media in acetone for 24 h. The powders were then dried and pressed into pellets. The pellets were heated at 1100 °C for 24 h at a heating rate of 5 K min^{-1}, ground into fine powder using the same milling media in acetone and dried. Once dried the powders were pressed into pellets and sintered at 1150 °C for 12 h. After cooling the samples were polished using diamond to a 1 μm level. The density of the samples was found to be >95% by the application of Archimedes's principle.

Table 1. Unit-Cell Parameters Derived from X-ray Powder Diffraction Data (Errors in the Final Digit Are Shown in Brackets)

composition	*a* (Å)	*b* (Å)	*c* (Å)	*V* (Å^3)
$SrBi_2Ta_2O_9$	5.510(5)	5.500(7)	24.976(15)	756.9(18)
$SrBi_{1.99}La_{0.01}Ta_2O_9$	5.499(5)	5.490(10)	24.942(8)	752.9(23)
$SrBi_{1.98}La_{0.02}Ta_2O_9$	5.499(4)	5.491(6)	24.910(5)	752.2(15)
$SrBi_{1.95}La_{0.05}Ta_2O_9$	5.500(5)	5.491(8)	24.904(5)	752.1(19)
$SrBi_{1.90}La_{0.1}Ta_2O_9$	5.492(5)	5.494(3)	24.872(11)	750.5(14)
$SrBi_{1.85}La_{0.15}Ta_2O_9$	5.511(2)	5.496(2)	24.879(8)	753.5(9)
$SrBi_{1.80}La_{0.20}Ta_2O_9$	5.511(5)	5.495(5)	24.921(2)	754.7(15)

To confirm phase assemblage, samples were examined as powders using a Siemens D500 powder diffractometer with weighted Cu K-alpha radiation (1.5418 Å) and graphite monochromator. The patterns were collected over an angular range of 5−70° with a step size of 0.02 degrees and a 1 s per step counting rate. Grain structures from freshly prepared fracture surfaces were examined using a CAMSCAN Mk2 electron microscope using secondary electron emission and an accelerating voltage of 20 kV. The microstructure was further were examined using a Philips EM430 transmission electron microscope with an accelerating voltage of 300 kV. Samples were ground to 25 μm and then thinned to electron transparency using a Gatan Duo Mill ion-beam thinner.

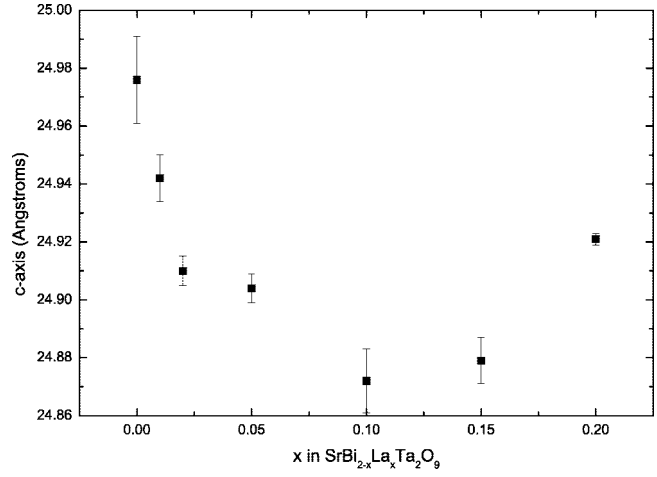

Figure 3. Plot of *c*-axis length against *x* in $SrBi_{2-x}La_xTa_2O_9$, data shown in Table 1.

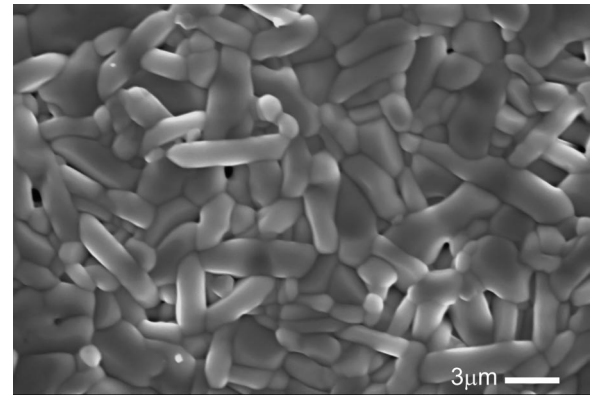

Figure 4. Secondary electron image from $SrBi_{1.9}La_{0.1}Ta_2O_9$ showing the elongated grains, typical of these systems.

(16) Noguchi, Y.; Miyayama, M.; Oikawa, K.; Kamiyama, T. *J. Appl. Phys.* **2004**, *95*, 4261–4266.
(17) Shi, H.; Lin, Y.; Tang, T.-A. *Solid State Commun.* **2005**, *135*, 304–307.
(18) Miyayama, M.; Noguchi, Y. *J. Eur. Ceram. Soc.* **2005**, *25*, 2477–2482.
(19) Mata, J.; Duran, A.; Martinez, E.; Siqueiros, J. M.; Heiras, J. *Mater. Res. Soc. Symp. Proc.* **2005**, *848*, 307–312.
(20) Noguchi, Y.; Miyayama, M. *Mater. Res. Soc. Symp. Proc.* **2004**, *784*, 419–427.

Table 2. Results from the Refinement of $SrBi_{1.8}La_{0.2}Ta_2O_9$[a]

name	Wyckoff site	*x*	*y*	*z*	$100U_{iso}$	frac
			Amam[b]			
Sr	4a	0.75	0.7491(9)	0.000000	0.71(4)	0.841(47)
Bi	4a	0.75	0.7491(9)	0.000000	0.71(4)	0.143(43)
La	4a	0.75	0.7491(9)	0.000000	0.71(4)	0.016(5)
Sr	8b	0.75	0.2645(6)	0.29889(6)	1.98(4)	0.080(24)
Bi	8b	0.75	0.2645(6)	0.29889(6)	1.98(4)	0.828(21)
La	8b	0.75	0.2645(6)	0.29889(6)	1.98(4)	0.092(2)
Ta	8b	0.75	0.2458(6)	0.08515(5)	0.296(17)	1.0000
O1	4a	0.75	0.2883(8)	0.000000	1.087(70)	1.0000
O2	8b	0.75	0.1935(5)	0.15838(11)	1.773(57)	1.0000
O3	8b	0.0	0.0	0.74955(11)	0.878(26)	1.0000
O4	8b	0.0	0.0	0.93072(7)	0.730(31)	1.0000
O5	8b	0.0	0.0	0.41693(10)	1.555(38)	1.0000
			$A2_1am$[c]			
Sr	4a	0.0504(22)	0.2494(9)	0.000000	0.89(4)	0.764(47)
Bi	4a	0.0504(22)	0.2494(9)	0.000000	0.89(4)	0.213(42)
La	4a	0.0504(22)	0.2494(9)	0.000000	0.89(4)	0.024(5)
Sr	8b	0.5469(18)	0.7652(6)	0.20109(6)	2.06(5)	0.118(23)
Bi	8b	0.5469(18)	0.7652(6)	0.20109(6)	2.06(5)	0.794(21)
La	8b	0.5469(18)	0.7652(6)	0.20109(6)	2.06(5)	0.088(2)
Ta	8b	0.5486(14)	0.7465(5)	0.41464(6)	0.350(22)	1.0000
O1	4a	0.0624(25)	0.7121(9)	0.000000	0.873(79)	1.0000
O2	8b	0.5291(16)	0.6976(7)	0.34216(10)	1.725(61)	1.0000
O3	8b	0.8025(22)	0.0032(16)	0.25060(10)	0.849(31)	1.0000
O4	8b	0.7995(15)	0.9987(13)	0.06933(7)	0.709(34)	1.0000
O5	8b	0.817760	0.9823(10)	0.58332(9)	1.064(47)	1.0000

[a] Models use Amam and $A2_1am$ space group symmetry, respectively. The errors in the final digits are given in the brackets and are the esd's reported by GSAS. The wR_p and R_p values obtained from refinement using a model based on I4/mmm were 0.0393 and 0.0403, indicating poorer refinement than the models above. [b] $SrBi_{1.8}La_{0.2}Ta_2O_9$; $wR_p = 0.0183$, $R_p = 0.0257$. [c] $SrBi_{1.8}La_{0.2}Ta_2O_9$; $wR_p = 0.0172$, $R_p = 0.0248$.

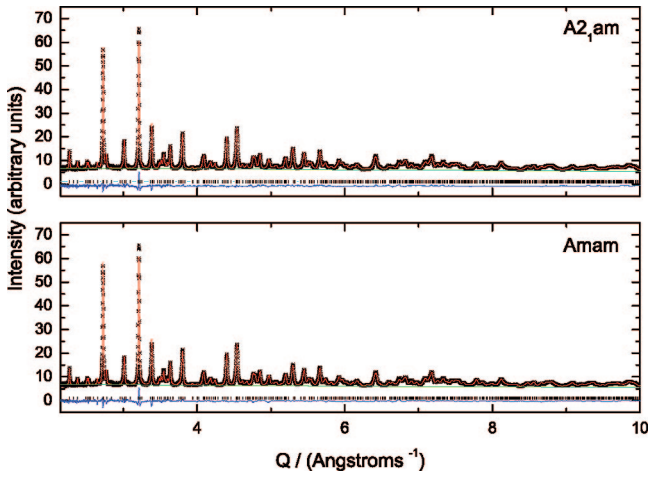

Figure 5. Graphical results from the refinement of the recorded neutron data using $A2_1am$ and Amam symmetries as model.

Variable-temperature capacitance and dielectric loss measurements were collected using a HP 4284a LCR meter at 1, 10, 100, 250, and 1000 kHz, between 10K and 1073K. At temperatures below 300 K, an Oxford Instruments 1020 Cryocooler and above 300 K a Carbolite tube furnace were used to control the temperature.

Polarization-electric field (P-E) hysteresis loops were recorded with a computer controlled modified Sawyer−Tower circuit supplied with sinusoidal electric field of 50 Hz. The maximum electric field that could be applied was 4 kV, and all measurements were carried out at 298K on thinned samples.

Raman spectra were collected using a Renishaw InVia microscope with an incident radiation of 514.5 nm, coupled with a Rencam CCD detector operating in back-scattered geometry. Samples were collected at both room temperature, and at variable temperature in the range −60 to 180 °C, using a Linkam cooling/heating stage with optically flat glass windows. The CCD detector

Table 3. Bond Valence Summations (S_{ij}) for $SrBi_{1.8}La_{0.2}Ta_2O_9$ Using Amam and $A2_1am$ Symmetries[a]

model	site	fraction	length	error	no.	S_{ij}	error
Amam	A, Sr/Bi/La−O	0.841/0.143/0.016	2.548	0.006	1		
			2.982	0.006	1		
			2.7707	0.005	2		
			2.6142	0.0027	4		
			2.8493	0.003	4	2.334	0.021
	B, Bi/Sr/La−O	0.828/0.080/0.092	2.9715	0.0012	2		
			2.602	0.004	1		
			2.3482	0.0025	2		
			2.2641	0.0024	2	2.741	0.019
	C, Ta−O	1	2.142	0.0015	1		
			1.8537	0.0033	1		
			1.9783	0.0022	2		
			1.9713	0.0022	2	5.195	0.033
$A2_1am$	A, Sr/Bi/La−O	0.764/0.213/0.024	2.972	0.007	1		
			2.559	0.007	1		
			2.705	0.013	1		
			2.837	0.012	1		
			2.617	0.007	2		
			2.604	0.008	2		
			2.766	0.006	2		
			2.953	0.006	2	2.336	0.049
	B, Bi/Sr/La−O	0.794/0.118/0.088	2.883	0.009	1		
			2.626	0.005	1		
			2.293	0.008	1		
			2.235	0.005	1		
			2.342	0.009	1		
			2.357	0.008	1	2.679	0.052
	C, Ta−O	1	2.148	0.0015	1		
			1.8352	0.0033	1		
			1.973	0.008	1		
			1.99	0.008	1		
			1.969	0.009	1		
			1.979	0.009	1	5.220	0.092

[a] The summations are in close agreement with each other and are both indicative of reliable refinements.

decreases in efficiency below 200 cm^{-1}, with an observed decrease in intensity the lower the shift, thus preventing some modes from being visible in the spectra.

Time-of-flight powder neutron diffraction data were collected on $SrBi_2Ta_2O_9$ and $SrBi_{1.8}La_{0.2}Ta_2O_9$ using the POLARIS diffractometer at the UK pulsed spallation neutron source ISIS, Rutherford Appleton Laboratory.[21,22] For each composition studied, approximately 10 g of powdered sample were loaded into a thin-walled, cylindrical vanadium sample can and diffraction data collected for between ∼185 μA h (equivalent to ∼1 h of neutron beamtime). Summed and normalized data collected in backscatter bank C (high resolution bank) over the time-of-flight range ∼2000 to 19 995 μs (corresponding to a range in Q of ∼2.15 to 11.2 $Å^{-1}$) were analyzed by the Rietveld Method using the GSAS suite of software[23] with the EXPGUI toolkit.[24]

Results and Discussion

Structural and Microstructural Characterization. *X-Ray Diffraction and Scanning Electron Microscopy.* X-ray powder diffraction traces, shown in Figure 2, collected from the synthesized powders before sintering did not reveal the presence of any second phases and all peaks could be indexed

(21) Smith, R. I.; Hull, S.; Armstrong, A. R. In *Epdic 3, Pts 1 and 2−Proceedings of the 3rd European Powder Diffraction Conference*, Vienna, Austria, Sept 25−28, 1994; Trans Tech Publications: Stafa-Zurich, Switzerland, 1994; Vol. 166, pp 251256.
(22) Smith, R. I.; Hull, S. *User Guide for the Polaris Powder Diffractometer at ISIS Rutherford Appleton Laboratory*; ISIS Rutherford Appleton Laboratory: Oxford, U.K., 1997.
(23) Larson, A. C.; Von Dreele, R. B. *General Structure Analysis System (GSAS)*; LANL Report LAUR 86-748Los Alamos National Laboratory: Los Alamos, NM, 2000.
(24) Toby, B. H. *J. Appl. Crystallogr.* **2001**, *34*, 210–213.

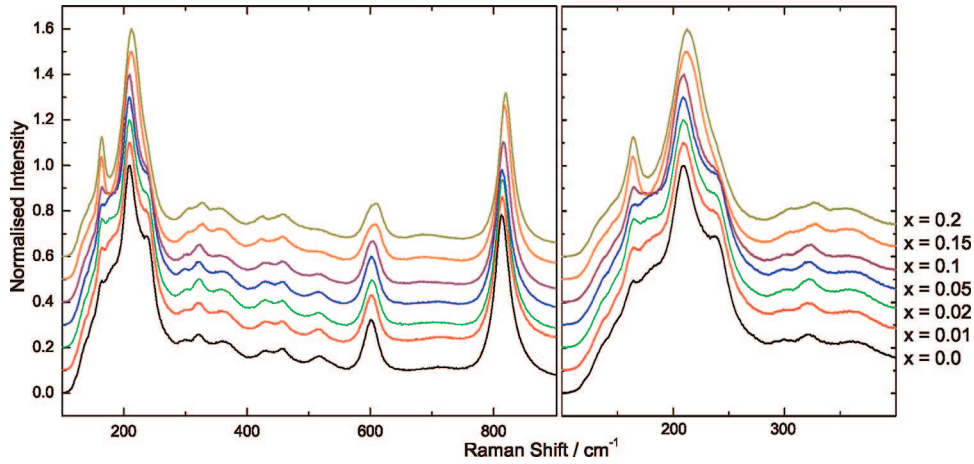

Figure 6. Room-temperature Raman spectra collected from the series $SrBi_{2-x}La_xTa_2O_9$ with $x = 0.0$, 0.01, 0.02, 0.05, 0.1, 0.15, and 0.2. The spectra have been normalized to the peak at 210 cm^{-1} the plot on the left is the complete range of data collected and the plot on the right is a magnification of the region 100−400 cm^{-1} more clearly illustrating the change in from $A2_1am$ to Amam symmetry as x increases.

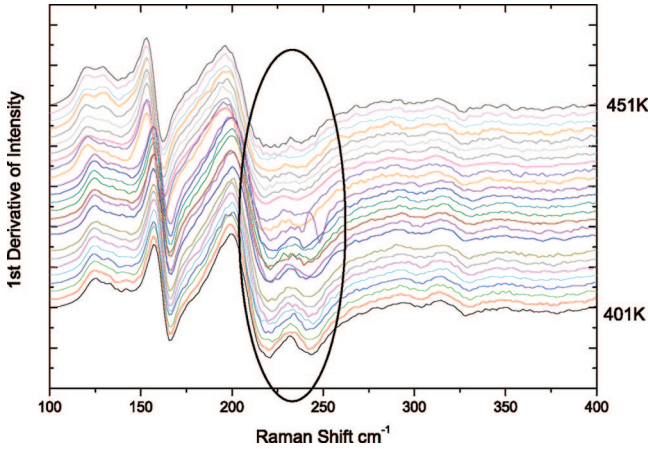

Figure 7. Variable-temperature Raman spectra recorded for $SrBi_{1.9}La_{0.1}Ta_2O_9$. The data have been plotted as the first derivative to highlight the change from $A2_1am$ to Amam symmetry.

using an orthorhombic cell of an $n = 2$ Aurivillius compound with A-centered symmetry, i.e. $A2_1am$ or Amam. The unit-cell parameters of all synthesized compounds are listed in Table 1. The lattice parameters do not vary significantly with x since the ionic radius of La^{3+} is close to that of Bi^{3+} (∼0.13 nm[25,26]) in similar co-ordination. However, the unit cell volume decreases marginally from $0 < x < 0.1$ and increases at $x > 0.1$, Figure 3. Non linearity in the unit-cell volume vs x indicates that the system does not conform to Vegards law and that there is a phase transition, presumably from $A2_1am$ to Amam, at $x \approx 0.1$.

Scanning electron microscopy of freshly fractured sintered pellets showed the grain structure to be consistent with a high density. An example image is shown in Figure 4. The acicular grains are typical of the crystal morphology expected for an orthorhombic layer-structure in which the c (layered axis) constitutes a more difficult growth direction compared with a and b. The average size of the grains was ∼1−2 μm in the thinner c-direction and ∼5 μm in the a- and b-directions. [27]

Neutron Diffraction. Rietveld refinements were carried out using two models based on $A2_1am$ and Amam space group symmetry for neutron diffraction data from $SrBi_2Ta_2O_9$ and $SrBi_{1.8}La_{0.2}Ta_2O_9$ samples. These samples were chosen as it was anticipated that $SrBi_2Ta_2O_9$ would refine as the $A2_1am$ phase, typical of an $n = 2$ ferroelectric Aurivillius compound whereas $SrBi_{1.8}La_{0.2}Ta_2O_9$ was most likely to have the orthorhombic paraelectric, structure with Amam symmetry at room temperature. In the early stages of refinement a Le-Bail fit was used to determine the best space group symmetry match to the recorded data. However, this proved to be inadequate to confirm symmetry, as the conditions limiting possible reflections for both space groups are identical. To determine structure and therefore space group symmetry, full Rietveld refinement was undertaken using the unit-cell sizes, and peak profiles determined in the Le-Bail fit. The results from the refinement are shown in Table 2. Statistically, it is not easy to determine which model best describes the system under examination and when the differences between the models and the recorded data are compared they are well within the expected error. Examples of the graphical results from refinement are shown in Figure 5, illustrating the equivalency of fit for the Amam and the $A2_1am$ space groups. The bond valence summations for both models are shown in Table 3.

It was concluded therefore that refinements of neutron diffraction data from $SrBi_{1.8}La_{0.2}Ta_2O_9$ and $SrBi_2Ta_2O_9$ were insensitive to the small difference between the Amam and $A2_1am$ symmetries. To differentiate between the two potential space groups, Raman spectroscopy was employed where it was anticipated that the loss of centrosymmetry on cooling through the Amam−$A2_1am$ phase transition should result in new active modes.

Raman Spectroscopy. Raman spectra were collected as a function of composition across the $SrBi_{2-x}La_xTa_2O_9$, Figure

(25) Shannon, R. D.; Prewitt, C. T. *Acta Crystallogr., Sect. B* **1969**, *25*, 925–946.
(26) Shannon, R. D. *Acta Crystallogr., Sect. A* **1976**, *32*, 751–767.
(27) Reaney, I. M.; Damjanovic, D. *J. Appl. Phys.* **1996**, *80*, 4223–4225.

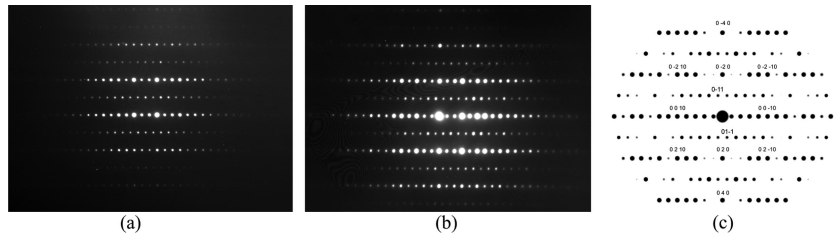

Figure 8. Electron diffraction pattern from the [100] zone axis in (a) $SrBi_2Ta_2O_9$ and (b) $SrBi_{1.8}La_{0.2}Ta_2O_9$ showing an identical superstructure in each composition; (c) a simulated kinematical diffraction pattern with peaks indexed. Indexed positions are shown for $01\bar{1}$ and $0\bar{1}1$ superstructure reflections.

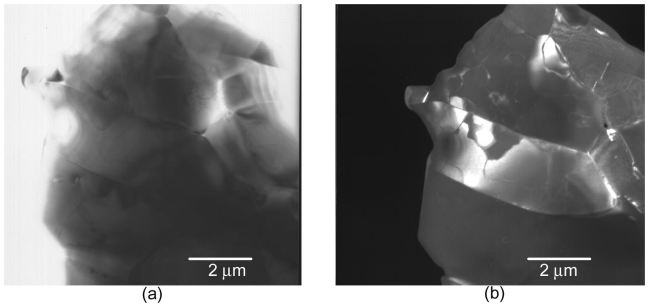

Figure 9. Transmission electron micrographs of $SrBi_2Ta_2O_9$, showing (a) a bright-field image the acicular grains and (b) a dark-field image taken obtained using the superlattice reflections arrowed in Figure 8; note the presence of orientational and translational domain variants.

Table 4. Change in Permittivity As Function of Lanthanide Concentration, Measured at 10 KHz (Errors in Measured Temperature Are Shown in Brackets)

composition	peak in permittivity (K)	relative permittivity at peak
$SrBi_2Ta_2O_9$	568(1)	360
$SrBi_{1.99}La_{0.01}Ta_2O_9$	555(1)	392
$SrBi_{1.98}La_{0.02}Ta_2O_9$	550(1)	290
$SrBi_{1.95}La_{0.05}Ta_2O_9$	510(1)	250
$SrBi_{1.90}La_{0.1}Ta_2O_9$	410(1)	270
$SrBi_{1.85}La_{0.15}Ta_2O_9$	246(2)	210
$SrBi_{1.80}La_{0.20}Ta_2O_9$	170(2)	135

6. Using the software previously published by Kroumova et al.,[28] SAM, it is possible to predict the potential modes for each of the 3 known symmetries adopted by $SrBi_2Ta_2O_9$.

$$A2_1am: \quad 22A_1 + 20A_2 + 20B_1 + 22B_2 \quad \text{total } 84$$

$$Amam: \quad 11A_{1g} + 13B_{1g} + 9B_{2g} + 8B_{3g} \quad \text{total } 41$$

$$I4/mmm: \quad 4A_{1g} + 2B_{1g} + 6E_g \quad \text{total } 12$$

The difference in the number of Raman active modes in between $A2_1am$ and Amam is 43. However, it is well-known that many such modes will overlap and the practical differences in recorded spectra from Amam and $A2_1am$ phases may well be slight. In this study, no attempt was made at precise mode assignment for the two orthorhombic phases. Some references are made to assignments based on the I4/mmm cell by previous researchers,[5,29] but in general, a comparative approach was utilized as a function of temperature and composition to determine the onset of the $A2_1am-Amam$ phase transition. It should be noted that bands at 167 and 181 cm^{-1} have lower intensities than anticipated because of detector efficiency decreasing below 200 cm^{-1}. Using the I4/mmm unit cell as a basis,[5,29] it is possible to assign modes to some of the observable peaks. The band at 160 cm^{-1} is assigned to an A1g mode present in phases which are centrosymmetric, i.e., Amam and I4/mmm. E_g modes, present in I4/mmm symmetry, between 200 and 400 cm^{-1} split to lower symmetry modes (A and B) in the $A2_1am$ and Amam structures. These are likely to be from the $Bi_2O_2^{2+}$ layers within the structure. Ta−O octahedral A1g modes, A1 when $A2_1am$ symmetry is adopted, give rise to bands at 600 and 810 cm^{-1}. The peak position of the TaO_6 at 810 cm^{-1} increased from 812 cm^{-1} for $SrBi_2Ta_2O_9$ to 819 cm^{-1} for $SrBi_{1.8}La_{0.2}Ta_2O_9$, presumably related to the decrease in ionic mass of the A-site in the perovskite blocks as La substitutes for Bi. Most importantly, the observation that the centrosymmetric, A1g band at 160 cm^{-1} increases sharply in intensity between two incremental lanthanum concentrations ($x = 0.1$ and $x = 0.15$), while at the same time the shoulder at 240 cm^{-1} disappears is characteristic of a change in symmetry, presumably between $A2_1am$ and Amam. The observation of a change in symmetry at $x \approx 0.1$ is consistent with the trends in unit cell volume shown in Figure 3.

Variable-temperature measurements were recorded for $SrBi_{1.9}La_{0.1}Ta_2O_9$, and $SrBi_{1.85}La_{0.15}Ta_2O_9$ through the expected $A2_1am-Amam$ phase transition, a plot of the first derivative of the recorded for $SrBi_{1.9}La_{0.1}Ta_2O_9$ is shown in Figure 7. The first derivative of the data is presented as it highlights the subtle changes in peak shape that arise from the change in symmetry between Amam and $A2_1am$. As temperature increases, a transition is observed at ~420 and ~250 K for $x = 0.1$ and 0.15, respectively, similar to that obtained from the $SrBi_{2-x}La_xTa_2O_9$ as a function of composition.

Transmission Electron Microscopy. Figure 8 shows the electron diffraction patterns with the beam parallel with a $[010]_o$ of $SrBi_2Ta_2O_9$ and $SrBi_{1.8}La_{0.2}Ta_2O_9$. The patterns in each case are identical and can be indexed according to an A-centered orthorhombic cell (either Amam or $A2_1am$) with the approximate lattice parameters listed in Table 1. Superstructure reflections arising from the unit cell doubling are arrowed and have qualitatively similar intensities in each case. Figure 9 shows a bright field TEM image of several grains in a $SrBi_2Ta_2O_9$ and the associated dark field image obtained using the systematic row of superstructure reflections of arrowed in Figure 8. The highlighted grain contains bright and dark regions which correspond to twin $[010]_o$ and $[100]_o$ 90° domain variants, respectively of the orthorhombic structure. Additionally, within the bright $[010]_o$ variant,

(28) Kroumova, E.; Aroyo, M. I.; Perez Mato, J. M.; Kirov, A.; Capillas, C.; Ivantchev, H.; Wondratschek, H. *Phase Transitions* **2003**, *76*, 155–170.
(29) Moret, M. P.; Zallen, R.; Newnham, R. E.; Joshi, P. C.; Desu, S. B. *Phys. Rev. B* **1998**, *57*, 5715–5723.

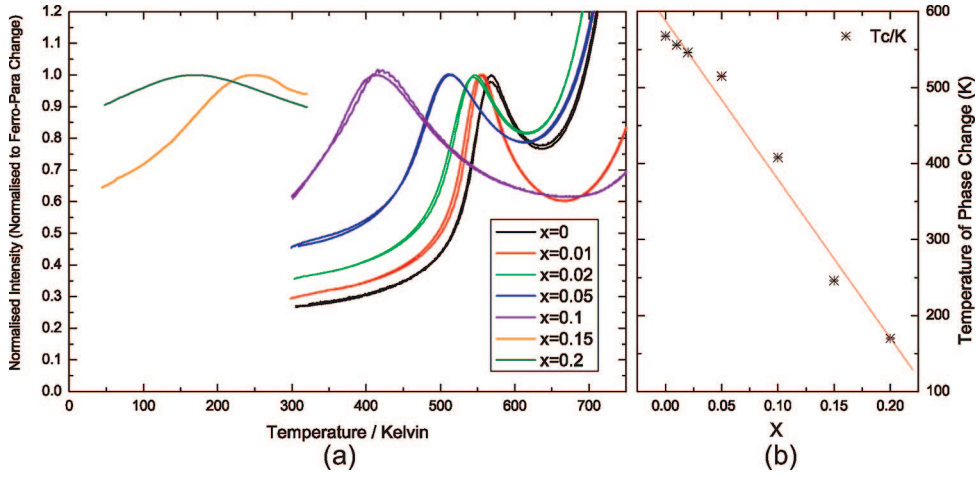

Figure 10. (a) Normalized plots of permittivity versus temperature for different values of x in $SrBi_{2-x}La_xTa_2O_9$, where the peak corresponds to the Amam to $A2_1am$ phase transition; (b) phase transition temperature as a function of x.

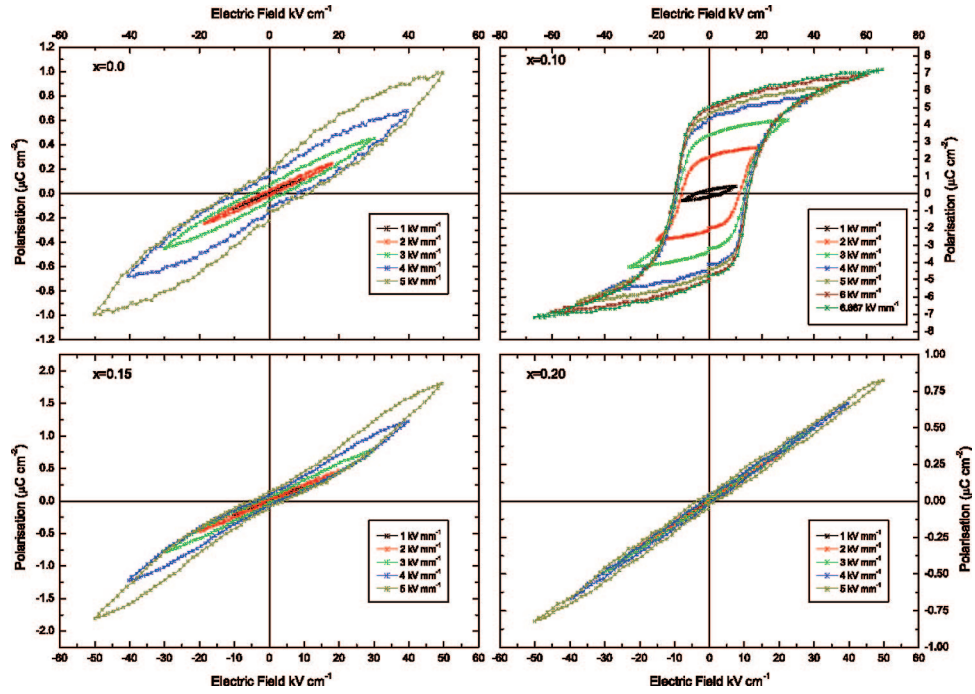

Figure 11. Ferroelectric hysteresis loops recorded for $SrBi_{2-x}La_xTa_2O_9$ at 298 K.

ribbonlike planar defects are observed (arrowed) that correspond to antiphase boundaries that have formed when two out of phase tilted regions impinge. Similar planar defects were also observed for the $SrBi_{1.8}La_{0.2}Ta_2O_9$ and similar images were observed for strontium bismuth titanate-based ceramics by Reaney et al. [8,27]

Electrical Measurements. *Relative Permittivity.* The relative permittivity as a function of temperature are shown in Table 4 and Figure 10. Substituting La for Bi has decreased the temperature of the ferroelectric−paraelectric phase transition (T_c) from 568 to 170 K, at $x = 0.2$ and the maximum permittivity (ε_r(max)) from 360 to 135. The value of 568 K agrees with that previously published by Almeida et al. [6] who studied single crystals of $SrBi_2Ta_2O_9$. The decrease in T_c and the ε_r(max) is most likely linked to the replacement of highly polarizable Bi^{3+} cations with less-polarizable La^{3+}. At low La concentrations, a second weak anomally in the permittivity as a function of temperature could be observed between 850 and 950 K which may be related to the phase transition from Amam to I4/mmm. However, the intensity of this peak reduced to zero as La concentration increased and could not therefore be used to monitor the onset of tilting in these samples.

Ferroelectric Hysteresis. Ferroelectric hysteresis loops recorded at room temperature for $SrBi_2Ta_2O_9$, $SrBi_{1.9}La_{0.1}Ta_2O_9$, $SrBi_{1.85}La_{0.15}Ta_2O_9$, and $SrBi_{1.8}La_{0.2}Ta_2O_9$ are shown in Figure 11. Four characteristic types of loops are observed. $SrBi_2Ta_2O_9$ to $SrBi_{1.95}La_{0.05}Ta_2O_9$, ($T_c$ values of ~568 and 510 K, respectively) did not exhibit saturated loops with evidence of only partial switching. For $SrBi_{1.9}La_{0.1}Ta_2O_9$ with $T_c \approx 410$ K, saturated hysteresis loops were obtained with a coercive field and remanent polarization of 15 kV cm^{-1} and 5 μC cm^{-1}, respectively, both lower than those reported for undoped $SrBi_2Ta_2O_9$,[16] possibly because of the reduction in spontaneous polarization by substituting La^{3+} for Bi^3. $SrBi_{1.85}La_{0.15}Ta_2O_9$ exhibits only partial switching

at room temperature. However, the ε_r (max) is broad at ~ 246 K with evidence that some of the sample is ferroelectric above room temperature. It is therefore suggested that part of the composition is ferroelectric at room temperature and is capable of being switched whereas a significant volume fraction of the sample is paraelectric. $SrBi_{1.8}La_{0.2}Ta_2O_9$, $T_c \approx 170$, exhibits a linear increase in polarization with field typical of a paraelectric phase.

General Discussion. La^{3+} and Bi^{3+} have similar ionic sizes (~0.13 nm[25,26]) but their polarizabilities differ markedly with the lone pair Bi^{3+} ion being generally considered as ferroelectrically active in perovskites and related materials. Suarez et al.[4] empirically demonstrated that the tolerance factor for the perovskite blocks has a linear relationship with the onset temperature of T_c for a broad range of Sr, Ca, Ba, and Pb-based Aurivillius compounds. They postulated that the tolerance factor controlled the onset temperature of octahedral rotations in the Aurivillius family which in turn were strongly coupled to the spontaneous polarization. Hence, the anomalously high T_c of compounds such as $CaBi_2Nb_2O_9$ and $Ca_2Bi_4Ti_5O_{18}$ (>1250 K) in comparison to $Bi_4Ti_3O_{12}$ (~950 K) could be rationalized. In the $SrBi_{2-x}La_xTa_2O_9$ series, tolerance factor effectively remains the same and only the average polarizability decreases with increasing La concentration. From the structural and electrical data presented, it is evident that T_c decreases with La concentration despite tolerance factor remaining largely constant in direct contrast to the crystallochemical plots first presented by Suarez et al.[4] Moreover, the Amam intermediate, tilted paraelectric, orthorhombic phase is still retained at room temperature even for $SrBi_{1.8}La_{0.2}Ta_2O_9$, whose T_c occurs at 170 K. It is evident therefore that the crystallochemical relationship between tolerance factor and T_c is not entirely related to the onset of octahedral tilting and is more complex than Suarez et al.[4] previously considered. In a recent publication, Hyatt et al.[30] reported that as T_c decreases the temperature interval between the onset of tilting (T_{Amam}) and that of ferroelectricity (T_{A21am}) increases with decreasing ferroelectric T_c. Therefore, the temperature dependence of T_{Amam} with composition is markedly different than that of T_{A21am}. One of the compelling arguments made by Suarez et al.[4] is that if Ca, Sr, and Ba bismuth niobate and titanates are considered, the high T_c of, for example, $CaBi_2Nb_2O_9$ and $Ca_2Bi_4Ti_5O_{18}$, may be explained only by the lower tolerance of factor of these compound and not on the polarizability and coordination of the constituent ions. Low t increases the onset temperature for tilt, which is coupled strongly to the onset of spontaneous polarization, and T_c increases. However, the increase in $T_{Amam} - T_{A21am}$ demonstrated by Hyatt et al.[30] as T_c decreases indicates that coupling of the onset of tilting to the spontaneous polarization is significantly weaker as Tc decreases. Moreover, the data presented in this article shows that it can be completely decoupled by the substitution of La for Bi in the $SrBi_{2-x}La_xTaO_9$ series. The general relationship between and T_c and tolerance factor illustrated by Suarez et al.[4] may therefore only apply for Aurivillius phases whose T_{Amam} and T_{A21am} are in close proximity and are able to couple. Such compounds invariably have high T_c. For lower T_c compounds, coupling is insignificant and T_c is more likely to be controlled by the average polarizability of the constituent ions in their requisite coordinations. Any relationship between tolerance factor and T_c for low T_c compounds is therefore coincidental.

(30) Hyatt, N. C.; Reaney, I. M.; Knight, K. S. *Phys. Rev. B* **2005**, *71*, 024119.

Conclusions

La-doped SBT compositions have been fabricated in which the ferroelectric phase transition (T_{A21am}) decreased with increasing La concentration but the temperature of the octahedral tilt transition (T_{Amam}) presumably remained largely unchanged. The data confirm that octahedral tilting and the onset of ferroelectricity are not strongly coupled in all Aurivillius compounds as previously postulated. Instead, coupling is proposed to be strong in high T_c compounds, with the onset of ferrroelectricity enhanced in low t compounds such as $CaBi_2Nb_2O_9$, but becomes progressively weaker as T_c decreases accompanied by a commensurate increase in the temperature interval $T_{(Amam)} - T_{(A2_1am)}$. Any relationship between tolerance factor and T_c for low T_c compounds is therefore considered coincidental.

Acknowledgment. We wish to acknowledge the funding by the Council for Central Laboratories of the Research Councils (CCLRC) for access to the ISIS neutron facility.

CM800475Z